Long-Lived Electronic Coherence of Iodine in the Condensed Phase: Sharp Zero-Phonon Lines in the B↔X Absorption and Emission of I2 in Solid Xe

ARTICLE *in* JOURNAL OF PHYSICAL CHEMISTRY LETTERS · JUNE 2012

Impact Factor: 7.46 · DOI: 10.1021/jz300651v

4 AUTHORS, INCLUDING:

Eero Hulkko
University of California, Irvine
14 PUBLICATIONS **75** CITATIONS
SEE PROFILE

Johan Lindgren
University of Jyväskylä
7 PUBLICATIONS **9** CITATIONS
SEE PROFILE

Toni Kiljunen
University of Jyväskylä
32 PUBLICATIONS **381** CITATIONS
SEE PROFILE

THE JOURNAL OF PHYSICAL CHEMISTRY Letters

Letter

pubs.acs.org/JPCL

Long-Lived Electronic Coherence of Iodine in the Condensed Phase: Sharp Zero-Phonon Lines in the B↔X Absorption and Emission of I_2 in Solid Xe

Eero Hulkko,* Johan Lindgren, Toni Kiljunen, and Mika Pettersson

Nanoscience Center, Department of Chemistry, University of Jyväskylä, P.O. Box 35, FI-40014, Jyväskylä, Finland

Supporting Information

ABSTRACT: Our study of B←X absorption of molecular iodine (I_2) isolated in a low-temperature crystalline xenon has revealed an exceptionally long-lived electronic coherence in condensed phase conditions. The visible absorption spectrum shows prominent vibronic structure in the form of zero-phonon lines (ZPLs) and phonon side bands (PSBs). The resolved spectrum implies weak interaction of the chromophore to the lattice degrees of freedom. The coherence extends past the vibrational period of the excited state molecule, unlike that observed in any condensed phase environment for I_2 so far. The ZP transitions from the relaxing B-state populations were resolved in the hot luminescence when the 532 nm laser was used for excitation.

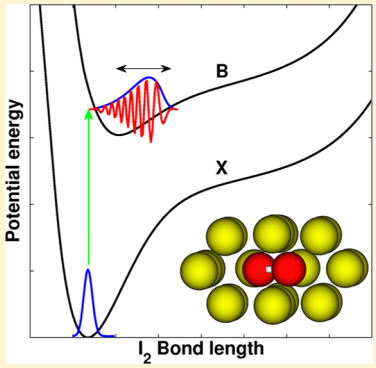

SECTION: Spectroscopy, Photochemistry, and Excited States

The visible absorption of I_2 is dominated by the $B(^3\Pi_u(0_u^+))\leftarrow X(^1\Sigma_g(0_g^+))$ transition as shown in the bottom spectrum of the Figure 1a, depicting the relative gas-phase molar absorption coefficients of different visible region transitions.[1] The I_2 absorption contains weaker overlapping contributions from two other electronic transitions: $C(^1\Pi_u(1_u))\leftarrow X$ and $A(^3\Pi_u(1_u))\leftarrow X$. Absorption from the ground state to the bound portion of the B-state is generally known to be highly structured in the gas phase, with very accurately determined rovibronic transitions.[2] In liquids,[3,4] clathrates,[5] or solid rare gases (RGs),[6,7] the I_2 B←X rovibronic fine structure collapses completely to a broad structureless Franck−Condon (F−C) envelope, due to fast electronic dephasing of the generated linear polarization $P^{(1)}$.[8] In the time-dependent semiclassical descriptions, this is understood as the decay of the many-body quantum correlation function prior to a wavepacket recursion on the excited I_2 B-state.[7] Numerous time-domain femtosecond pump−probe studies utilizing the B-state in solid RGs have shown that *vibrational* coherences[9] generated in this particular state are relatively long-lived (∼3−5 ps). Thus the vibrational state structure and the potential form of the B-state can be seen in the wavepacket dynamics. It has been shown that the gas-phase B-state of I_2 is fairly well preserved in the RGs, apart from the typical dielectric solvation of the potential origin[6] and the strong "caging effect"[10] by the surrounding RG atoms. We show in this letter that the solid Xe environment for the I_2 is peculiar, because the linear absorption and emission spectroscopies show prominent vibronic structure in the form of zero-phonon lines (ZPLs) and phonon side bands (PSBs), probing the *electronic* coherence[9] between X and B states. We are not aware of any previous observation of discrete vibronic structure in the B↔X spectrum of I_2 in the condensed phase.

The appearance of vibronic structure in the B←X absorption of I_2/Xe is shown in Figure 1a. Now we establish that the vibronic structures observed in the B←X absorption are sharp ZPLs with accompanying broader, higher energy, PSBs. Both types of transitions are common for molecules isolated in low-temperature solids.[11,12] ZPLs are electronic or vibrational transitions without the change of the phonon state ($\Delta n = 0$) of the surrounding environment. A PSB is formed when lattice modes of a solid environment are impulsively excited along with the impurity molecule or atom resulting in a simultaneous change of the phonon state ($\Delta n \neq 0$). Bimodal vibronic structure with a ca. 90 cm^{-1} B-state spacing becomes apparent in the 16000−18000 cm^{-1} region by cooling the crystalline I_2/Xe sample prepared at $T = 45$ K to $T = 10$ K (see Figure 1a). At the higher temperature of $T = 45$ K, only a hint of the vibronic structure remains visible on the smooth absorption background. By comparison with the low-resolution gas-phase absorption spectrum (Figure 1a, bottom), the vibronic structure is seen to appear in the low energy portion of the B-state.

As shown in the inset of Figure 1a, the strong temperature dependence and the relative positions of the two bands can be taken as evidence for the ZPL+PSB structure similar to other halogens in the lighter RGs.[13−16] This assignment can be

Received: May 22, 2012
Accepted: June 20, 2012
Published: June 20, 2012

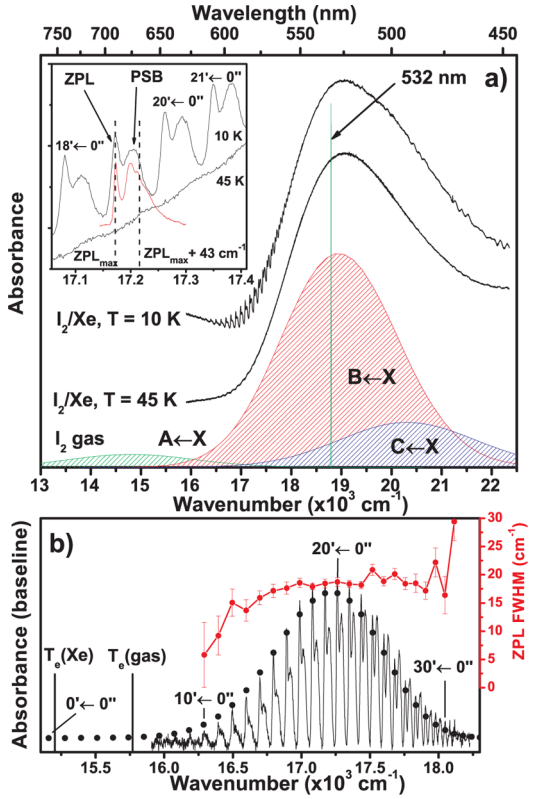

Figure 1. (a) Absorption spectra of I_2 in solid Xe at T = 10 K and T = 45 K. The gas-phase molar absorption coefficients of different I_2 electronic transitions from ref 1 (colored spectra) are given normalized to B←X maximum. Inset in panel a magnifies the vibronic structure in the I_2/Xe absorption spectra, showing the ZPL and PSB structures as a function of temperature. (b) The resolved ZPL region with suggested vibronic B←X transitions. The spectrum is obtained from the T = 10 K spectrum by removing the continuous absorption background by baseline correction. Black dots show the calculated transitions obtained using the spectroscopic parameters of this work (see Table 1), red dots are linewidths for the corresponding ZPLs in the energy spectrum. Note the scale for the ZPL fwhm on the right-hand side.

further confirmed by comparing the PSB distributions with previously measured PSBs in solid Xe. The red line in Figure 1a inset is a spin–orbit transition ($^2P_{1/2}$←$^2P_{3/2}$) of atomic I in solid Xe with a distinct ZPL and PSB.[17] The phonon contributions are qualitatively very similar in both cases as seen by shifting the atomic ZPL from its original position (near-IR) to coincide the arbitrarily selected molecular 19′← 0″ ZPL. Most of the PSB absorption falls within the highest observed single-phonon transition energy[18] (~43 cm^{-1}) from the ZPL (dashed lines), further indicating electron–phonon coupling as the source for the broad transitions.

Next, we will use the positions of the experimental ZPLs to characterize the excited state potential in solid Xe, and extract the spectroscopic parameters for the B-state potential. In Figure 1b we show the ZPL-region with suggested vibronic transitions and the estimated B-state potential minimum T_e(Xe) in comparison with the gas phase potential minimum T_e(gas).[2] The lowest energy ZPL in our absorption spectrum is located at ω = 16080 cm^{-1} (for complete list, see Supporting Information Table S1). In order to correctly assign the ZPLs, we varied the B-state vibrational numbering v' (v'← 0″), and solved the spectroscopic parameters for different numberings using a normal Birge–Sponer[19] analysis, including a second anharmonicity constant ($\omega_e y_e$) (see Supporting Information Figure S1 and Table S2). The experimental parameters were then compared to parameters obtained from molecular dynamics (MD) simulation of the B-state (unpublished results), which suggest significant reduction (−3.5 cm^{-1}) of the harmonic frequency (ω_e) in solid Xe from the gas phase value (see Table 1), similarly to Cl_2 in solid Ar.[15] By comparing the B-state T_e values with different ZPL numberings (Table S2) to the magnitude of the A-state solvation in solid Xe ($\Delta T_e(A)$ = −507 cm^{-1}),[20] which can be expected to be very similar, we can narrow the possible assignments of 16080 cm^{-1} ZPL as 9′–7′← 0″. In an overall agreement with the B-state MD simulation (ω_e reduction) and A-state solvation (≈500 cm^{-1}), we assign 16 080 cm^{-1} transition as 8′← 0″ (with ±1 uncertainty) and label the rest of the ZPLs accordingly. The B-state spectroscopic parameters with this assignment are listed in Table 1. The parameters give a reasonably accurate description of the ZPL energies throughout the observed ZPL region as shown by the black dots in Figure 1b. The largest absolute difference between calculated transitions and the maxima of experimental ZPLs is 7 cm^{-1}, which is much less than the line width of ZPLs (average 17.6 cm^{-1}).

Sharp ZPLs in the absorption spectrum of Figure 1 are a direct evidence of electronic coherences that outlive the I_2 vibrational period in the condensed phase. Linewidths of ZPLs range between 6 and 29 cm^{-1} as shown in Figure 1b (red dots). The linewidths are obtained by least-squares fitting the ZPLs with Lorentzian functions. The lower limit of the electronic dephasing time can be estimated from the linewidths using the relation[22]

$$\tau = \frac{1}{\pi c \Gamma} \qquad (1)$$

where τ is the dephasing time, and Γ is the Lorentzian width in units of cm^{-1}. The lower limits of electronic dephasing times range between 0.37 and 1.7 ps. Note that for I_2 in solid Kr or Ar, electronic coherence times are well below the vibrational period of the I_2 molecule (<300 fs).[23,24] Thus no vibronic

Table 1. Spectroscopic Parameters for the I_2 States X and B in Solid Xe[a]

I_2 state	ω_e ($\Delta\omega_e$)[b]	$\omega_e x_e$ ($\Delta\omega_e x_e$)[b]	$\omega_e y_e$ ($\Delta\omega_e y_e$)[b]	T_e (ΔT_e)[b]	method
B	120.2 (−5.1)	0.60 (−0.10)	−0.006 (0)	15200 (−570)	absorption
B[c]	121.7 (−3.5)	0.78 (+0.08)	0.001(+0.007)		MD
X[d]	210.26 (−4.24)	0.672 (+0.058)			Raman
X[e]	211.5 (−3.0)	0.640 (+0.026)			MD

[a]All values are in units of cm^{-1}. [b]Δ values calculated using the gas phase parameters: B-state from ref 2 and X-state from ref 21. [c]From Birge–Sponer analysis of calculated B-state energies (v' = 0–30) including a second anharmonicity constant ($\omega_e y_e$) obtained from MD simulated B-state potential at T = 50 K (unpublished results). [d]Previously reported values in solid Xe: ref 20: ω_e = 207, $\omega_e x_e$ = 0.7; ref 32: ω_e = 213.9, $\omega_e x_e$ = 0.67. [e]Averaged values from calculated Raman transitions v'' = 0–20 obtained from MD simulation at T = 50 K (unpublished results).

dx.doi.org/10.1021/jz300651v | J. Phys. Chem. Lett. 2012, 3, 1847–1852

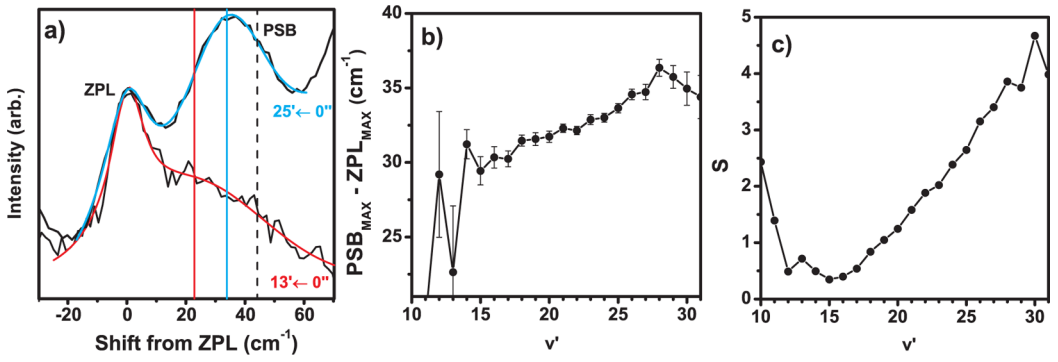

Figure 2. (a) Comparison of 13′← 0″ and 25′← 0″ ZPLs and PSBs. The *x*-axis is the shift from the respective ZPL maxima. (b) Difference of ZPL and PSB maxima as a function of B-state vibrational quantum v'. The difference is estimated from the maxima of combined least-squares fits of ZPLs (Lorentzian function) and PSBs (Gaussian function). The combined fits are shown with colored lines for the two transitions in panel a, with the respective PSB maxima marked with solid vertical lines. (c) The v'-dependence of the estimated phonon coupling strength *S*.

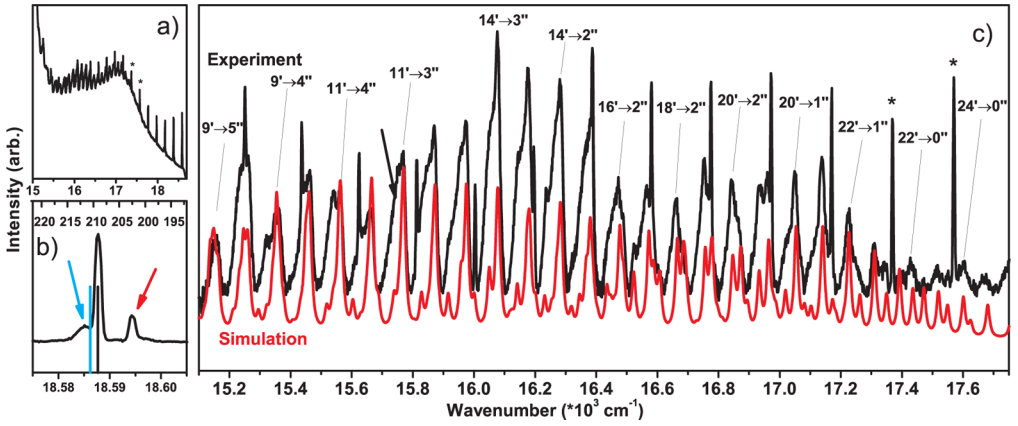

Figure 3. (a) Hot luminescence and resonance Raman transitions of I_2/Xe with 532 nm excitation. (b) High-resolution Raman fundamental transition 0″→1″ from the same sample. Top scale in panel b is the Stokes-side Raman shift. See text for explanation of the colored arrows and lines. (c) Baseline corrected emission spectrum in comparison with the simulated spectrum. Suggested vibronic B→X transitions have been marked in panel c.

structure in absorption can be observed for these systems. As stated, the electronic dephasing range must be considered as the lower limit, because we are not fully certain of the homogeneity of the ZPLs. We also note that the increase of linewidths (see Figure 1b) as a function of the B-state vibrational quantum is not monotonous, implying the possible presence of predissociation pathways.[16,25] The linewidths show notable kinks around 12′← 0″ and in the high energy region (v' > 23).

Many types of lattice vibrations can contribute to the PSBs: Xe lattice phonons[18,26,27] on one hand, and impurity-induced (pseudo)local phonons[15,28,29] on the other. In fact, the broad continuum background under the ZPLs in the absorption spectra (see Figure 1a, T = 10 K) can be considered to originate from higher-order (Δn > 1) phonon transitions that start overlapping with the next, higher energy, ZPL.[16] This is seen in the accumulation of the *unresolved* absorption background around ω>17500 cm^{-1} in Figure 1a. The *resolved* PSB distributions (clear PSB bands) located on top of the unresolved background are not constant in the observed range of ZPL transitions. The shape, the relative position, and the relative intensity of the resolved PSBs compared to the ZPLs are dependent on the excited vibrational state reached on the B-state (v'). The exact analysis of the PSBs, without the detailed knowledge of the phonon modes of the I_2/Xe system, is beyond the scope of this publication, but the qualitative trends in the phonon coupling can be obtained from the absorption spectrum. Figure 2a shows the spectral changes in the PSBs for two representative transitions: 13′← 0″ and 25′← 0″. The increase in the ZPL line width at the higher energies is clearly visible in the 25′← 0″ spectrum. Interestingly, the resolved PSBs show completely opposite behavior. The phonon bands become narrower with increasing v' and the resolved PSB linewidths are comparable to the ZPL linewidths at the highest observed transitions (near $v' \approx 30$, full width at half-maximum ($fwhm_{PSB}$) ≈ 20 cm^{-1}). The PSBs become more localized to the high energy end of the I_2/Xe phonon density (further from the ZPL) at higher energies. This behavior is shown in Figure 2b, showing the energy difference of resolved PSB maxima to the ZPL maxima as a function of B-state vibrational quantum. The observed trends can be understood either as more efficient coupling of the chromophore to the local high energy phonons with higher excitations[15] or as generation of coherent zone boundary phonon near the Debye-frequency (marked with dashed line in Figure 2a) of solid Xe similarly to solid Kr.[27]

The phonon coupling strength also shows increasing trend as a function of v' as shown in Figure 2c, depicting the Huang–Rhys coupling constants *S* obtained from the absorption spectrum of Figure 1a. The coupling constants have been calculated with a similar procedure as discussed in detail for Br_2 in solid Ar in ref 16, i.e.,

dx.doi.org/10.1021/jz300651v | J. Phys. Chem. Lett. 2012, 3, 1847–1852

$$S(\nu') = \ln\left(\sum_{n=0}^{\infty} \frac{I_n(\nu')}{I_0(\nu')}\right) \quad (2)$$

where the ratio in the brackets compares the intensity of the whole vibronic structure for respective ν' (ZPL+ PSB) to the intensity of corresponding ZPL. For $I_0(\nu')$, we used the area from Lorentzian fits of ZPLs, and for the $\sum I_n(\nu')$ the whole integrated area between two successive ZPL lines. This procedure takes into account the rising unresolved phonon background in Figure 1a. We also note that the validity of our procedure is limited to qualitative description of coupling strength, due to possible contributions from I_2 aggregates and I_2 molecules in different trapping sites to the continuous absorption background (see Figure 3b). The phonon coupling strength shows a qualitatively increasing trend at higher ν' excitations, but the increase of S at lower energies is quite unexpected. We suggest very fast predissociation to the repulsive part of another valence state as a possible phenomenon for the increased coupling strength near the B-state minimum.

Nonrelaxed hot luminescence[30] (B→X) and resonance Raman transitions of I_2 with 532 nm excitation (experimental laser spectrum is shown as green line in Figure 1a) in solid Xe at T = 10 K are shown in Figure 3. Note that the shown spectra are measured from the same matrix sample as in Figure 1. Sharp Raman transitions (with ca. 200 cm^{-1}spacing) are observable on the rising emission background extending up to Raman overtone 0″→18″ (≈15250 cm^{-1}). Two Raman overtones 0″→6″ and 0″→7″ are marked with asterisks to ease the identification of the Raman lines. The ground state Morse-parameters obtained from the positions of the Raman lines are listed in Table 1. With the 532 nm (18797 cm^{-1}) excitation, the unstructured emission is observable directly at lower energies from the laser line and develops a maximum near 17000 cm^{-1} (see Figure 3a). In the same energy region, we start to observe highly structured emissions with B-state energy spacing of ca. 90 cm^{-1}. The discrete hot luminescence (ZPLs) can be observed without difficulty in the ca. 17000−15000 cm^{-1} region. At the lower energies, detection of weak hot luminescence peaks is hampered by the strong relaxed emissions from the doubly spin-excited states[30] (I*−I*), which completely dominate the spectrum in the ca. 15000−14000 cm^{-1} region. However, the luminescence peaks can be weakly observed on top of the spin-excited emissions, and even extending to the lower energies. We could observe clear hot luminescence structures continuing at the end of our measurement range (13500 cm^{-1}), and we have no reason to believe that the luminescence peaks could not be observed even at lower energies.

Figure 3b shows the high-resolution Raman fundamental at T = 10 K. The fundamental region shows multiple transitions: A sharp transition at 209.3 cm^{-1} and a broader blue-shifted transition at 211.6 cm^{-1} (blue arrow). The two contributions are reproduced in our I_2/Xe samples nearly independently of sample preparation parameters (temperature, sample deposition rate). In addition to the two transitions, we observe a red-shifted transition at 202.7 cm^{-1} (red arrow). Our MD simulations (unpublished results) for the I_2-doped FCC Xe-lattice imply that the dominant sharp (instrument limited) transition belongs to a I_2 molecule in a double substitutional site in solid Xe (simulated frequency shown with a black line), and the broad blue-shifted line belongs to a site with an additional Xe vacancy (triple substitution, vacancy located at 90° angle to molecular bond axis, blue line). The red-shifted Raman line belongs to a small aggregate species $(I_2)_m$ in solid Xe, based on the analogous red-shifting of ≈10 cm^{-1} of fundamental frequency in small $(I_2)_m$ aggregates (m = 2−4) in solid Kr.[31] The extent of how much I_2 aggregates and different sites contribute to the emission and absorption is unclear. However, the ZPL structures are reproduced in absorption and emission spectra of purely monomeric matrices prepared at 10 K (only the sharp line and the blue-shifted line observed in high resolution Raman), and thus we rule out that the aggregate species is responsible for the ZPLs. Unfortunately, we have not been able to optimize the matrix preparation parameters at T = 10 K in a way that optically suitable matrices for high-quality absorption measurements could be produced.

The presence of ZPLs in absorption suggests that ZP transitions could also explain the vibrationally resolved structures in the hot luminescence. We note that ZPLs have been previously reported in the relaxed A→X emission of solid I_2/Xe.[32] Using the B-state potential obtained from the ZPLs in absorption, the laser line (532 nm) is expected to excite the vibrational state near v′ = 46 (presumably no longer a well-defined eigenstate of the B-state). We calculated the F−C factors (intensities) for the B→X emissions using the Morse parameters obtained in this work (see Table S2, Morse ν' = 8, without second anharmonicity correction, and Table 1 for the ground state), and the known r-dependent transition dipole moment function for the gas-phase B-state.[33] We note that inclusion of transitions from states $\nu' \geq 28$ would produce lines that are not observed in the experiment, thus only the transitions from the states ν' = 0−27 were calculated in our simulation. Gas-phase equilibrium distances ($r_{e,X}$ = 2.666 Å, $r_{e,B}$ = 3.024 Å)[21] were used in the spectral simulation. We used constant population for all calculated B-state vibrational states. Lorentzian line shape with a line width of 15 cm^{-1}, and the third-power intensity law were used to convolute the calculated F−C stick spectrum. Additional intensity scaling was introduced for adjusting the simulated spectrum better to the experimentally observed transitions, namely, the contributions of emitting states ν' = 23, 24, 25, 26, and 27 were multiplied by 5/6, 2/3, 1/2, 1/3, and 1/6, respectively. This procedure mimics the presumably fast relaxation of the higher vibrational states. Final transition energies of simulated ZPLs in emission were adjusted to their correct positions using the spectroscopic parameters listed in Table 1, including the second anharmonicity correction. The simulated result is the red spectrum in Figure 3c. In comparison with the simulation, we are showing the experimental emission spectrum (black line) where the unresolved emission background has been removed for clarity.

The simulation reproduces the positions of the experimentally observed sharp emissions (clear peaks in the spectrum) in a quantitative manner giving great confidence to the determined spectroscopic parameters. The simulation shows that the emissions are superpositions of multiple overlapping transitions that originate from various vibrational states in the B-state to the lowest levels in the ground state, mainly in the range of ν'' = 0−4. In this sense, the ZPL hot-luminescence behaves completely normally in the light of F−C factors, as has been already shown for the unstructured emission in RGs.[30] We note that our simulation will only reproduce the positions of sharp ZPLs in emission but not the broad unstructured hot luminescence (see Figure 3a). We have marked some of the resolved transitions in the spectra (more complete character-

dx.doi.org/10.1021/jz300651v | J. Phys. Chem. Lett. 2012, 3, 1847−1852

ization of the transitions can be found in the Supporting Information Table S3). Most notably, the simulation reproduces the change in the shape of the emissions. At higher energies (ca. 17200−16400) the doublet structures are well reproduced, and at lower energies (ca. 16300−15200) the emissions are more localized in the blue edge of the emission structures. However, the broad diffusive "wings" (marked with an arrow for 11′→3″) on the red-edges of the emissions in the low energy region are clearly not reproduced by the ZPL simulation. This is most likely due to fact that PSB contributions are neglected in our treatment. In emission, the PSB contributions are expected to appear in the red-energy side of the ZPLs, while in absorption, the PBSs appear in the blue sides of the ZPLs.

The key question is why ZPLs are present in a low-temperature crystalline I_2/Xe, but not in other condensed phase environments? We suggest a simple mechanistic reason: the large mass of the Xe and small mass difference of I_2 and Xe, and reasonably large double substitutional cavity of the I_2 inside the solid Xe lattice. The I_2 molecule excited to the B-state is not fully able to displace the surrounding cage Xe atoms during the expansion-contraction of the vibrational coordinate. The coupling of the molecule to lattice modes is therefore weak during the collision of the molecule and the caging Xe atoms. Thus the correlation function describing the time-evolution of excited state wavepacket upon absorption is not fully dephased during the first expansion, giving the system time to make recursion before the phase correlation between the electronic states is lost irreversibly. Such wavepacket recursions have been shown by simulations to occur during a Raman process in large I_2−Xe_{18} clusters, and interestingly predicted to be enhanced in solid Xe lattice.[34]

The existence of ZPLs and PSBs in the B←X transition opens up interesting new possibilities to study the I_2/Xe system. For example, steering and controlling the coherences between I_2 and the Xe lattice modes using ultrafast pulse trains similar to a Br_2 in solid Ar can be easily envisaged.[35] The unexpectedly long electronic coherence times in the condensed phase between the X and the B states in the linear polarization $P^{(1)}$ suggest that higher order polarization (namely $P^{(3)}$) could also exhibit long electronic coherences between the states that should be easily observable using, for example, TRCARS.[28,29] The ability to directly see the B-state potential and the vibrational structure in absorption and emission of the I_2/Xe opens up possibilities to reinvestigate the predissociation and vibrational relaxation for this system, previously only seen indirectly through pump−probe measurements in the condensed phase.

EXPERIMENTAL METHODS

Prior to gaseous sample preparation, solid I_2 was purified by several freeze−pump−thaw cycles in a high vacuum system. A gas mixture with an I_2/Xe ratio of 1/2600 was then prepared to a 5 dm^3 glass bulb at room temperature. Xenon gas (Aga, 99.999%) was purchased from the manufacturer and used without additional purification. Solid I_2/Xe matrix samples were prepared on a 150 μm sapphire substrate kept inside a closed-cycle He cryostat (ADP cryogenics). The cryostat was initially evacuated to a high vacuum ($\sim 10^{-6}$ mbar), and the substrate was cooled to low temperatures; the gaseous sample was then sprayed on the low-temperature substrate by continuous deposition until the notable "reddish" color of I_2 was visually detected (typically 0.07—0.13 mmol/min). Matrices were prepared at temperatures of T = 45 K and T = 10 K. Stokes branch resonance Raman measurements of I_2/Xe matrices were carried out with our home-built backscattering Raman spectrometer with ∼1 cm^{-1} and ∼5 cm^{-1} resolutions using a frequency doubled single-mode CW Nd:YAG laser (Alphalas) operating at 532 nm. A Peltier-cooled CCD detector (Andor Newton) combined with a 50 cm focal length spectrograph (Acton SpectraPro 2500i) was used for detection of the Raman and emission signals. The Rayleigh line of the laser was suppressed using an edge filter (Semrock). Spectral response of the detection system was corrected using a calibrated tungsten-halogen lamp. The system was carefully calibrated using a combination of calibration lines obtained from liquid toluene-acetonitrile-standard and previously obtained high accuracy calibration curves for the I_2/Kr system.[31] Detection for the absorption measurements was carried out using the Raman setup described above. Measurements were done in a transmission geometry using a stable white-light light emitted diode (LED) as the light source.

ASSOCIATED CONTENT

Supporting Information

(Table S1) Positions and widths of the ZPLs and PSBs in absorption. (Figure S1) Birge−Sponer analysis with different B-state vibrational numberings. (Table S2) Spectroscopic parameters with different B-state vibrational numberings. (Figure S2) Enlargement of Figure 3c. (Table S3) Positions of simulated hot luminescence transitions. This material is available free of charge via the Internet at http://pubs.acs.org

AUTHOR INFORMATION

Corresponding Author

*E-mail: eero.hulkko@jyu.fi.

Notes

The authors declare no competing financial interest.

ACKNOWLEDGMENTS

This work was financially supported by the Academy of Finland. E.H. and M.P. were supported by the Academy decision No. 122620, and T.K. and J.L. were supported by the decision No. 124974. E.H. would like to acknowledge financial support from the Department of Chemistry at the University of Jyväskylä. We would like thank V.A. Apkarian for stimulating and helpful discussions.

REFERENCES

(1) Tellinghuisen, J. Least-Squares Analysis of Overlapped Bound-Free Absorption Spectra and Predissociation Data in Diatomics: The C($^1\Pi_u$) State of I_2. *J. Chem. Phys.* **2011**, *135*, 054301.

(2) See, for example, Steinfeld, J. I.; Zare, R. N.; Jones, L.; Lesk, M.; Klemperer, W. Spectroscopic Constants and Vibrational Assignment for the B $^3\Pi_{0u}^+$ State of Iodine. *J. Chem. Phys.* **1965**, *42*, 25−33.

(3) Sension, R. J.; Strauss, H. L. Comparison of Experiment and Theory for the Resonance Raman Spectrum of I_2 in Solution. I. The Raman Excitation Profile of I_2 in *n*-Hexane. *J. Chem. Phys.* **1986**, *85*, 3791−3806.

(4) Xu, J.; Schwentner, N.; Chergui, M. Femtosecond Dynamics of I_2(B $^3\Pi_{0u}^+$) in Liquids from Resonance Raman Spectra. *J. Chem. Phys.* **1994**, *101*, 7381−7387.

(5) Senekerimyan, V.; Goldschleger, I.; Apkarian, V. A. Vibronic Dynamics of I_2 Trapped in Amorphous Ice: Coherent Following of Cage Relaxation. *J. Chem. Phys.* **2007**, *127*, 214511.

(6) Bargheer, M.; Gühr, M.; Dietrich, P.; Schwentner, N. Femtosecond Spectroscopy of Fragment-Cage Dynamics: I_2 in Kr. *Phys. Chem. Chem. Phys.* **2002**, *4*, 75−81.
(7) Ovchinnikov, M.; Apkarian, V. A. Condensed Phase Spectroscopy from Mixed-Order Semiclassical Molecular Dynamics: Absorption, Emission, and Resonant Raman Spectra of I_2 Isolated in Solid Kr. *J. Chem. Phys.* **1996**, *105*, 10312−10331.
(8) Mukamel, S. *The Principles of Nonlinear Optical Spectroscopy*; Oxford University Press: New York, 1995.
(9) For distinction of "electronic" and "vibrational" coherence, and a recent review of the previous ultrafast studies in this field, see, for example, Gühr, M.; Bargheer, M.; Fushitani, M.; Kiljunen, T.; Schwentner, N. Ultrafast Dynamics of Halogens in Rare Gas Solids. *Phys. Chem. Chem. Phys.* **2007**, *9*, 779−801 and references therein.
(10) Apkarian, V. A.; Schwentner, N. Molecular Photodynamics in Rare Gas Solids. *Chem. Rev.* **1999**, *99*, 1481−1514.
(11) Rebane, K. K. Purely Electronic Zero-Phonon Line as the Foundation Stone for High Resolution Matrix Spectroscopy, Single Impurity Molecule Spectroscopy, Persistent Spectral Hole Burning. *J. Luminesc.* **2002**, *100*, 219−232.
(12) Andrews, L., Moskovits, M., Eds. *Chemistry and Physics of Matrix-Isolated Species*; Elsevier: Amsterdam, 1989.
(13) Bondybey, V. E.; Fletcher, C. Photophysics of Low Lying Electronic States of Cl_2 in Rare Gas Solids. *J. Chem. Phys.* **1976**, *64*, 3615−3620.
(14) Bondybey, V. E.; Bearder, S. S.; Fletcher, C. Br_2 B $^3\Pi(0_u^+)$ Excitation Spectra and Radiative Lifetimes in Rare Gas Solids. *J. Chem. Phys.* **1976**, *64*, 5243−5246.
(15) Ovchinnikov, M.; Apkarian, V. A. Mixed-Order Semiclassical Dynamics in Coherent State Representation: The Connection Between Phonon Sidebands and Guest-Host Dynamics. *J. Chem. Phys.* **1998**, *108*, 2277−2284.
(16) Ibrahim, H.; Gühr, M.; Schwentner, N. Valence Transitions of Br_2 in Ar Matrices: Interaction with the Lattice and Predissociation. *J. Chem. Phys.* **2008**, *128*, 064504.
(17) Pettersson, M.; Nieminen, J. Spin-Orbit Transitions ($^2P_{1/2}\leftarrow{}^2P_{3/2}$) of Iodine and Bromine Atoms in Solid Rare-Gases. *Chem. Phys. Lett.* **1998**, *283*, 1−6.
(18) Lurie, N. A.; Shirane, G.; Skalyo, J., Jr. Phonon Dispersion Relations in Xenon at 10 K. *Phys. Rev. B* **1974**, *9*, 5300−5306.
(19) Hollas, J. M. *Modern Spectroscopy*; Wiley: West Sussex, U.K., 2007.
(20) Macler, M.; Nicolai, J.-P.; Heaven, M. C. Electronic Spectroscopy and Energy Transfer Pathways of Matrix Isolated Iodine. *J. Chem. Phys.* **1989**, *91*, 674−682.
(21) Diatomic Constants for $^{127}I_2$. In *NIST Chemistry WebBook, NIST Standard Reference Database Number 69*; Data compiled by Huber, K. P.; Herzberg, G.; National Institute of Standards and Technology: Gaithersburg, MD; http://webbook.nist.gov (retrieved April 3, 2012).
(22) Skinner, J. L. Theory of Pure Dephasing in Crystals. *Annu. Rev. Phys. Chem.* **1988**, *39*, 463−478.
(23) Bihary, Z.; Karavitis, M.; Apkarian, V. A. Onset of Decoherence: Six Wave-Mixing Measurements of Vibrational Decoherence on the Excited Electronic State of I_2 in Solid Argon. *J. Chem. Phys.* **2004**, *120*, 8144−8156.
(24) Segale, D.; Karavitis, M.; Fredj, E.; Apkarian, V. A. Quantum Coherent Dissipation: A Glimpse of the "Cat". *J. Chem. Phys.* **2005**, *122*, 111104.
(25) Batista, V. S.; Coker, D. F. Nonadiabatic Molecular Dynamics Simulation of Photodissociation and Geminate Recombination of I_2 Liquid Xe. *J. Chem. Phys.* **1996**, *105*, 4033−4054.
(26) Leese, J. G.; Horton, G. K. Two-Phonon Raman Scattering of Light in Rare Gas Crystals. *J. Low Temp. Phys.* **1979**, *35*, 205−220.
(27) Gühr, M.; Bargheer, M.; Schwentner, N. Generation of Coherent Zone Boundary Phonons by Impulsive Excitation of Molecules. *Phys. Rev. Lett.* **2003**, *91*, 085504.
(28) Karavitis, M.; Apkarian, V. A. Vibrational Coherence of I_2 in Solid Kr. *J. Chem. Phys.* **2004**, *120*, 292−299.
(29) Kiviniemi, T.; Aumanen, J; Myllyperkiö, P.; Apkarian, V. A.; Pettersson, M. Time-Resolved Coherent Anti-Stokes Raman-Scattering Measurements of I_2 in Solid Kr: Vibrational Dephasing on the Ground Electronic State at 2.6−32 K. *J. Chem. Phys.* **2005**, *123*, 064509.
(30) Almy, J.; Kizer, K.; Zadoyan, R.; Apkarian, V. A. Resonant Raman, Hot and Cold Luminescence of Iodine in Rare Gas Matrixes. *J. Phys. Chem. A* **2000**, *104*, 3508−3520.
(31) Hulkko, E.; Kiljunen, T.; Kiviniemi, T.; Pettersson, M. From Monomer to Bulk: Appearance of the Structural Motif of Solid Iodine in Small Clusters. *J. Am. Chem. Soc.* **2009**, *131*, 1050−1556.
(32) Böhling, R.; Langen, J.; Schurath, U. A−X and A′−X Progressions in Dissociative Excitation of Matrix-Isolated I_2: Rare Gas Effect on Lifetimes and Intensities. *Chem. Phys.* **1989**, *130*, 419−432.
(33) Lamrini, M.; Bacis, R.; Cerny, D.; Churassy, S.; Crozet, P.; Ross, A. J. The Electronic Transition Dipole Moment of the $B0_u^+\rightarrow X0_g^+$ Transition in Iodine. *J. Chem. Phys.* **1994**, *100*, 8780−8783.
(34) Jungwirth, P.; Fredj, E.; Gerber, R. B. Ultrafast Quantum Dynamics and Resonance Raman Spectroscopy of Photoexcited I_2(B) in Large Argon and Xenon Clusters. *J. Chem. Phys.* **1996**, *104*, 9332−9339.
(35) Ibrahim, H.; Héjjas, M.; Schwentner, N. Tracing, Amplifying, and Steering Chromophore-Bath Coherences by Ultrashort Pulse Trains. *Phys. Rev. Lett.* **2009**, *102*, 088301.